Oligothiophene Nanorings as Electron Resonators for Whispering Gallery Modes

Gaël Reecht,[1] Hervé Bulou,[1] Fabrice Scheurer,[1] Virginie Speisser,[1] Bernard Carrière,[1] Fabrice Mathevet,[2] and Guillaume Schull[1,*]

[1]*IPCMS de Strasbourg, UMR 7504 (CNRS—Université de Strasbourg), 67034 Strasbourg, France*

[2]*Laboratoire de Chimie des Polymères, UMR 7610 (CNRS—Université Pierre et Marie Curie), 75252 Paris, France*

(Received 29 August 2012; published 29 January 2013)

Structural and electronic properties of oligothiophene nanowires and rings synthesized on a Au(111) surface are investigated by scanning tunneling microscopy. The spectroscopic data of the linear and cyclic oligomers show remarkable differences which, to a first approximation, can be accounted by considering electronic state confinement to one-dimensional boxes having, respectively, fixed and periodic boundary conditions. A more detailed analysis shows that polythiophene must be treated as a ribbon (i.e., having an effective width) rather than a purely 1D structure. A fascinating consequence is that the molecular nanorings act as whispering gallery mode resonators for electrons, opening the way for new applications in quantum electronics.

DOI: 10.1103/PhysRevLett.110.056802 PACS numbers: 73.22.−f, 68.37.Ef, 73.61.Ph, 82.35.Cd

Whispering galleries, such as the dome of St Paul's Cathedral in London [1], are intriguing structures conveying waves on a curved path. For closed-loop galleries, wave resonances appear when an integer number of wavelengths matches the perimeter of the resonator. These whispering gallery modes (WGMs) exist for all types of waves, and numerous applications emerged, from guided propagation of radio waves in the ionosphere [2,3] to confinement of light in optical WGM resonators [4–8]. For WGMs to exist, the coherence length of the waves must exceed the perimeter of the resonator, and the walls must efficiently reflect the waves. Circular walls of several meters, present in many monuments around the world, fulfill these conditions for acoustic waves [1]. For optical waves, micrometer resonators of various shapes supporting WGMs were designed [5]. In this case, the reflections at the outer wall rely on the total internal reflection at the medium-air boundary. More recently, whispering galleries were built for plasmons [9] and neutrons [10] and WGMs predicted for antihydrogen atoms [11]. While future electronic devices may highly benefit from this concept in charge transport, no whispering gallery effect for electrons has been evidenced so far. For electrons, a WGM resonator must be a nanoscale closed-curved conductive structure, reflecting electronic waves at its boundaries. One-dimensional (1D) extended molecules have recently attracted tremendous interest because of potential use as electrical nanowires [12–14]. The electronic structure of these oligomers can be approximated by a (nearly) free electron gas confined to a 1D box [15,16]. Here we use the intrinsic flexibility of a conjugated molecular wire, oligothiophene, to confine these electronic states in nanorings. The electronic properties of these rings are energetically and spatially resolved using scanning tunneling microscopy. This study reveals molecular resonances with homogeneous ring-shape spatial repartition whose diameter increases with energy, in agreement with the formalism describing WGMs [17].

The experiments were performed with an Omicron scanning tunneling microscope (STM) operated at 4.6 K in ultrahigh vacuum. Au(111) samples and chemically etched W tips were prepared by Ar^+ bombardment and annealing. 5,5″-Dibromo-2,2′:5′,2″-terthiophene (DBrTT) molecules [Fig. 1(a)] purchased from Sigma-Aldrich were evaporated from a Ta crucible. The Au(111) samples were heated at 400 K during the deposition and at 550 K for 30 min after to induce the on-surface polymerization [18] of the molecules [Fig. 1(a)]. The data shown correspond to a coverage of approximately 0.1 monolayer [19]. Differential conductance spectra (maps) were acquired using lock-in detection with a modulation frequency of 740 Hz and a root-mean-square modulation amplitude of

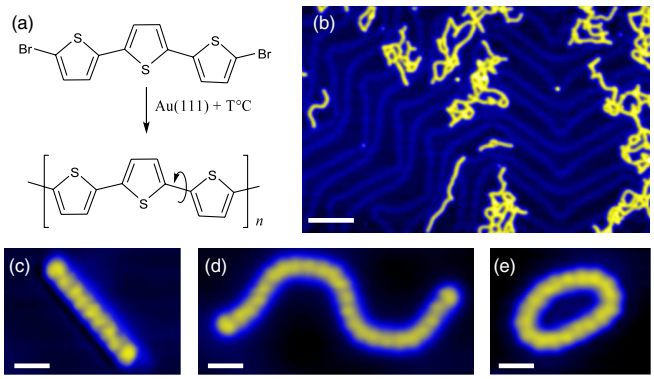

FIG. 1 (color online). (a) Sketch of the on-surface polymerization reaction of DBrTT on Au(111). (b) Large scale topographic STM image ($I = 100$ pA and $V_{sample} = 0.1$ V) and close-up views (c)–(e) of various oligothiophene structures resulting from the polymerization reaction. The white scale bars correspond 5 nm (b) and 1 nm (c)–(e).

10 (25) mV. All spectroscopic data were recorded at *constant height* to prevent artifacts linked to the trajectory of the STM tip.

A STM image of oligothiophene wires is shown in Fig. 1(b). High-resolved images of individual strands [Figs. 1(c)–1(e)] reveal intramolecular structures spaced by ≈ 0.38 nm, matching the distance measured between thiophene bases in oligothiophene [20–22]. In contrast to poly(*p*-phenylene) [16,23], which generally adopts a linear conformation, oligothiophene has the intrinsic ability to fold [20–22] because of the monomer's pentagonal geometry. Successive thiophene units can adopt two conformations: one where the sulfur atoms are opposite to each other and a second where they are on the same side of the wire. While the former leads to linear strands [Fig. 1(c)], the latter leads to bended molecular wires [Fig. 1(d)]. Close-ended cyclic oligomers [24] of different diameters also naturally form on the surface [Fig. 1(e)]. We will see below that, despite these folds, the electronic conjugation is preserved along the wires. Consequently, oligothiophene is an ideal candidate for electrical atomic-scale wires requiring high flexibility. On-surface polymerization, which was never used before to create thiophene-based polymers, allows synthesizing and studying *pure* thiophene macrocycles for the first time here. This method avoids solubilizing side groups, mandatory for syntheses in solution [24], which usually affect the conformations and electronic properties of oligothiophene.

To see how the closed-loop architecture of the rings impacts their electronic properties, a comparison with open-ended wires is mandatory. Figures 2(a) and 2(g) respectively display STM topographic images of a linear and a cyclic $N = 12$ oligothiophene (with N the number of thiophene bases). Differential conductance (dI/dV) spectra [Figs. 2(b) and 2(h)] identify the lowest unoccupied molecular orbitals (LUMOs) for the linear and cyclic structures. While the intensities of the conductance peaks vary as a function of tip position along the linear wires [e.g., Fig. 2(b)], the spectra remain unchanged along the cyclic structure. The number and the energy of the resonances are different for the two oligomers. Fitting the data with Gaussian distributions [green lines in Fig. 2(b) and 2(h)] reveals that the resonances have similar widths (≈ 0.4 eV). Details of the fitting procedure are available in Ref. [25]. Figures 2(c)–2(f) and 2(i)–2(k) show differential conductance maps acquired at constant height for the linear [cyclic] wire at voltages corresponding to maxima in the spectrum of Fig. 2(b) and 2(h). For the LUMO + n orbital, the conductance maps reveal $n + 1$ bright lobes along the linear wire, explaining the changes in the dI/dV spectra with tip position. This behavior can be understood from the confinement of states to a one-dimensional box as for oligothiophene adsorbed on NaCl [15]. For the cyclo-[12]-thiophene, the conductance maps reveal a different behavior. For the three considered orbitals, a uniform ring

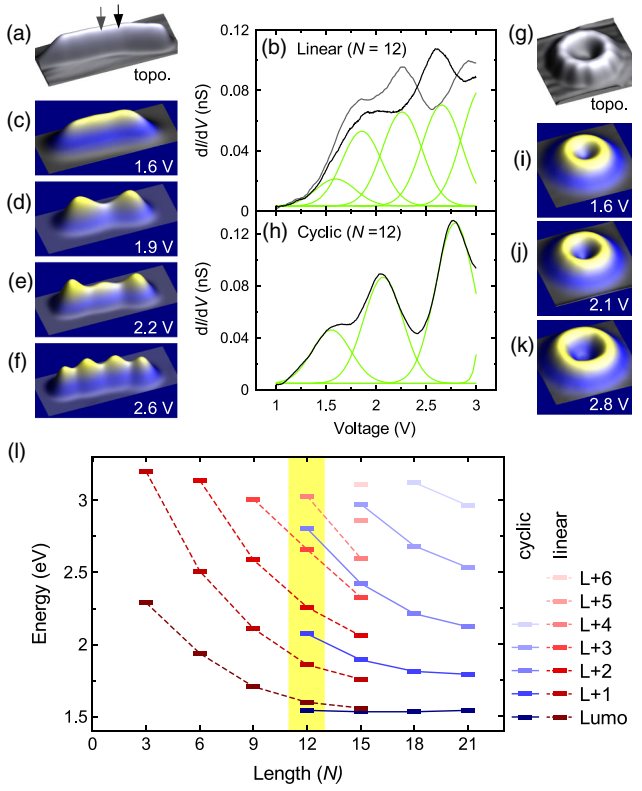

FIG. 2 (color online). (a) Topographic STM image ($I =$ 100 pA and $V_{\text{sample}} = 0.1$ V, 6.6×2.4 nm^2) and (b) constant height differential conductance spectra (set point: $I = 5$ pA and $V_{\text{sample}} = 1$ V) of a linear-[12]-thiophene. The gray and black spectra correspond to two positions of the tip on top of the wire [see gray and black arrows in (a)]. Light gray (green) lines are Gaussian function fits. (c)–(f) Constant height conductance maps acquired at voltages corresponding to maxima in (b). The same data were acquired for a cyclo-[12]-thiophene: (g) topographic STM image (2.8×2.8 nm^2), (h) constant height differential conductance spectra acquired on top of the wire, and (i)–(k) constant height conductance maps acquired at voltages corresponding to maxima in (h). No resonances were resolved at negative sample voltages. (l) Molecular state energies as a function of oligomer lengths for linear- (dashed red lines) and cyclo- (full blue lines) [N]-thiophene ([12]-thiophene wires are shaded [highlighted in yellow]).

(i.e., without nodes) is observed, whose diameter strikingly increases with the energy of the state. Spectroscopic data as a function of N [Fig. 2(l)] reveal a downward shift in energy and a reduction of the energy gaps between resonances when N increases for both linear and cyclic oligomers. This is the signature of electron delocalization [26], definitely evidencing the conjugated nature of the oligomers.

Figure 2(l) also confirms that the orbitals of linear and cyclic oligomers of equal length do not match. This apparent discrepancy finds its origin in the close-ended nature of the cyclo-[N]-thiophene resonances which must be treated with periodic boundary conditions [27]. This has two important consequences. (i) States exist only when an

integer multiple of the wavelength matches the length of the cyclic structures (half wavelength for the linear wires). Consequently, the wave numbers of linear- and cyclo-[N]-thiophenes are given, respectively, by $k = l\frac{\pi}{L}$ and $\bar{k} = l\frac{2\pi}{L}$, where l is the quantum state number and L the delocalization length [25]. (ii) Contrary to open-ended wires where wave functions vanish at the boundaries, the $l = 0$ resonance exists. The energy of this state is invariant with N, as experimentally observed [i.e., LUMO of the cyclic oligomers in Fig. 2(l)]. Figure 3(a) displays the deduced dispersion data for linear- and cyclo-[N]-thiophene for $N = 12$ and 15. The lines in Fig. 3(a) correspond to fits with a 1D tight-binding expression (see details in Ref. [25]). The overall shape of the dispersion curves is very similar for the two conformations, in agreement with the fact that the electronic properties of conjugated oligomers essentially derive from their length [26].

A close inspection of Fig. 3(a) reveals small, yet measurable, differences between the dispersion curves of the linear and cyclic structures. Unlike linear chains where the dispersion is length independent, the dispersion gets stronger with decreasing N for cyclo-[N]-thiophenes. This behavior, as well as the increased radius of the orbitals of the cyclic oligomers with energy [Figs. 2(i)–2(k)], can be accounted for by considering polythiophene as a 2D ribbon rather than a 1D wire. In this framework, the wave function of an electron of effective mass m^* moving in an annular potential $V(r)$ is given in polar coordinates by $\psi(\vec{r}) = R(r)Y(\theta)$, where $R(r) = \frac{u(r)}{\sqrt{(r)}}$ and $Y(\theta)$ are, respectively, the radial and angular parts and satisfy

$$-\frac{\hbar^2}{2m^*}\frac{d^2u(r)}{dr^2} + \left[V(r) + \frac{\hbar^2}{2m^*}\frac{1}{r^2}\left(l^2 - \frac{1}{4}\right)\right]u(r) = \epsilon u(r), \tag{1}$$

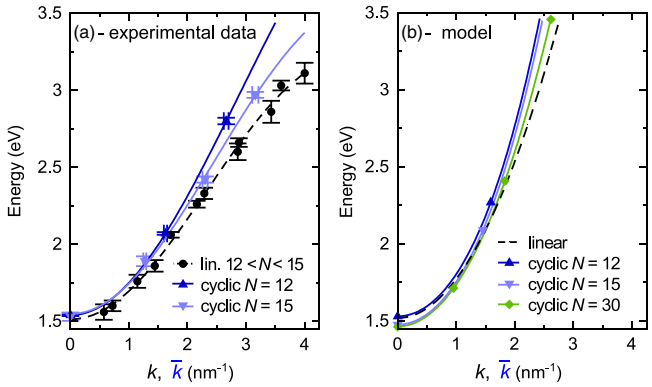

FIG. 3 (color online). Experimental (a) and calculated (b) dispersion data for linear and cyclic oligomers. The connecting lines correspond to fits with a 1D tight-binding expression. In (b) the parabolic dispersion of an infinite wire is represented (dashed lines). Details about the fits and the error bars are provided in Ref. [25].

$$\frac{d^2Y(\theta)}{d\theta^2} = -l^2Y(\theta), \tag{2}$$

where ϵ is the energy. The general solution of Eq. (2) being $Y(\theta) = a\exp(il\theta) + b\exp(-il\theta)$, l must be an integer to fulfill the periodic boundary conditions.

Equation (1) is the quantum expression of a wave equation whose solutions are 2D WGMs. The resemblance between a classical and a quantum representation of WGMs has been highlighted recently for a spherical (3D) symmetry [17]. For the 2D case, one defines the effective potential as

$$V_{\text{eff}}(r) = V(r) + \frac{\hbar^2}{2m^*}\frac{1}{r^2}\left(l^2 - \frac{1}{4}\right),$$

where $V(r)$ depends on the nature of the wave (acoustic, optic, electronic, etc.) and the geometry of the resonator, while $l^2 - \frac{1}{4}$ is common to all types of waves and accounts for centrifugal forces (except for $l = 0$ where the force is directed toward the center of the ring). Figure 4(a) represents the radial part of the state probability density $|R(r)|^2$ for $l = 0$, 1, and 2 calculated from Eq. (1) by using a Numerov procedure [28]. For $l \neq 0$, centrifugal forces modify the potential and produce a shift of the wave functions towards the outer wall with increasing l. This effect explains the increased radius of the nanoring's orbitals with energy observed in experimental conductance maps [Figs. 2(i)–2(k)]. For high values of l, a change of the inner wall radius has little influence on the position of the resonances, as expected for WGMs [3,29,30]. Finally, the $l = 0$ mode is localized to the inner wall. This surprising effect is linked to the 2D nature of the nanorings, and is therefore not observed in 3D resonators where the additional potential term is proportional to $l(l + 1)$.

Figure 4(b) represents the state probability density $|\psi(\vec{r})|^2$ in 3D for a given set of parameters (a, b). These maps reveal the $\cos(2l\theta)$ modulated nature of waves for $l \neq 0$ [31], in apparent discrepancy with the uniform rings observed experimentally [Fig. 4(c)]. However, since there is no privileged phase origin, the Hamiltonian having no explicit angle dependence, all combinations of (a, b) are equally possible, leading to the uniform rings reported in the experimental maps.

In our model, the height of the potential (5.2 eV) and the effective electron mass ($0.15m_e$) are deduced experimentally [25]. The left and the right borders of the potential [Fig. 4(a)] are adjusted to reproduce the radial spread of the experimental orbitals [Fig. 4(c)]. An effective width of 7 Å is estimated for polythiophene using this procedure. Figure 3(b) displays the dispersion curves of cyclic ($N = 12$, 15, 30) wells for these parameters together with the limit case of a linear wire with infinite potential [32]. Qualitatively, the behavior is the same as for the experiment: the dispersion of the ring's orbitals is larger than for the linear counterpart, and decreases as N increases. Eventually, the dispersion of linear and cyclic wells merges

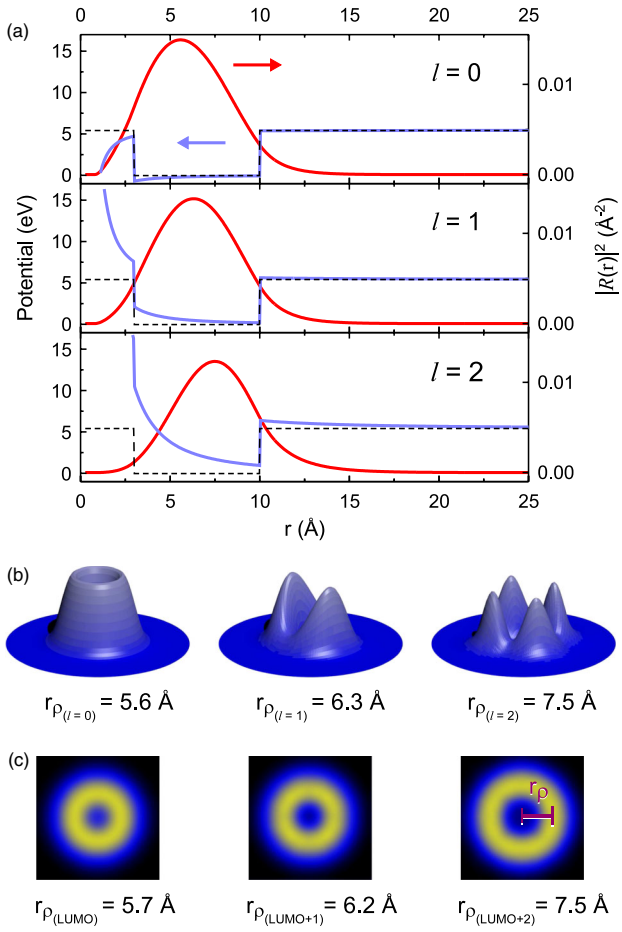

FIG. 4 (color online). (a) Finite square potential $V(r)$ (black dashed lines), effective potential $V_{\text{eff}}(r)$ [light gray (blue) lines], and WGM probability density [dark gray (red) lines] for $l = 0$, $l = 1$, and $l = 2$ modes. (b) 3D representations of the calculated WMG probability density for the $l = 0$, $l = 1$, $l = 2$ modes and for $(a, b) = (0.25, 0.75)$. (c) Constant height differential conductance maps of the cyclic-[12]-thiophene (2.8×2.8 nm^2) at energies of the LUMO, LUMO + 1, and LUMO + 2. Experimental and calculated representations are at the same scale. r_ρ is the radius defined as the distance from the center to the maxima of the circular resonances.

for infinitely long wires. Quantitatively, the model overestimates the dispersions, and the shapes of the curves are different. A more realistic description of the potential is likely to improve the agreement but would lack the simplicity of the square potential model.

Despite the simple form of the potential, our 2D model reproduces the experimental observations with good accuracy and shows that oligothiophene nanorings are resonators for electronic WGMs. A fascinating consequence of this effect is the confinement of high-energy orbitals to the outer perimeter of the nanorings, which also has important consequences in the scope of future applications: modes localized at the outer wall are more likely to couple adjacent cycles than modes confined to the inner wall. Thanks to this effect, a chain of cycles would act as a nanoscale electron energy high-pass filter. We speculate that molecular rings made of carbone nanotube slices [33] would possibly fulfill this objective.

We thank F. Charra and L. Limot for stimulating discussions, and J.-G. Faullumel and M. Romeo for technical support. The Agence National de la Recherche, Contract No. TRANSMOL ANR-2010-JCJ-1004, the Région Alsace, and the International Center for Frontier Research in Chemistry (FRC) are acknowledged for financial support.

*guillaume.schull@ipcms.unistra.fr

[1] Lord Rayleigh, *The Theory of Sound* (McMillan, London, 1878), Vol. 2, pp. 115–117.
[2] K. G. Budden and H. G. Martin, Proc. R. Soc. A **265**, 554 (1962).
[3] N. Carrara, M. T. De Giorgio, and P. F. Pellegrini, Space Sci. Rev. **11**, 555 (1970).
[4] C. Liu and J. A. Golovchenko, Phys. Rev. Lett. **79**, 788 (1997).
[5] K. J. Vahala, Nature (London) **424**, 839 (2003).
[6] F. Vollmer and S. Arnold, Nat. Methods **5**, 591 (2008).
[7] V. S. Ilchenko and A. B. Matsko, IEEE J. Sel. Top. Quantum Electron. **12**, 15 (2006).
[8] G. C. Righini, Y. Dumeige, P. Féron, M. Ferrari, G. N. Conti, D. Ristic, and S. Soria, Riv. Nuovo Cimento **34**, 435 (2011).
[9] C.-H. Cho, C. O. Aspetti, M. E. Turk, J. M. Kikkawa, S.-W. Nam, and R. Agarwal, Nat. Mater. **10**, 669 (2011).
[10] V. V. Nesvizhevsky, A. Y. Voronin, R. Cubitt, and K. V. Protasov, Nat. Phys. **6**, 114 (2010).
[11] A. Y. Voronin, V. V. Nesvizhevsky, and S. Reynaud, Phys. Rev. A **85**, 014902 (2012).
[12] S. Ho Choi, B. Kim, and C. D. Frisbie, Science **320**, 1482 (2008).
[13] L. Lafferentz, F. Ample, H. Yu, S. Hecht, C. Joachim, and L. Grill, Science **323**, 1193 (2009).
[14] G. Schull, T. Frederiksen, M. Brandbyge, and R. Berndt, Phys. Rev. Lett. **103**, 206803 (2009).
[15] J. Repp, P. Liljeroth, and G. Meyer, Nat. Phys. **6**, 975 (2010).
[16] S. Wang, W. Wang, and N. Lin, Phys. Rev. Lett. **106**, 206803 (2011).
[17] D. Pluchon, B. Bêche, N. Huby, and E. Gaviot, Opt. Commun. **285**, 2247 (2012).
[18] L. Grill, M. Dyer, L. Lafferentz, M. Persson, M. V. Peters, and S. Hecht, Nat. Nanotechnol. **2**, 687 (2007).
[19] A monolayer corresponds to saturation of the surface with DBrTT molecules deposited at room temperature. In this case, the molecules form close-packed 2D assemblies.
[20] H. Kasai, H. Tanaka, S. Okada, H. Oikawa, T. Kawai, and H. Nakanishi, Chem. Lett. **31**, 696 (2002).
[21] B. Grévin, P. Rannou, R. Payerne, A. Pron, and J. P. Travers, J. Chem. Phys. **118**, 7097 (2003).
[22] A. Bocheux, I. Tahar-Djebbar, C. Fiorini-Debuisschert, L. Douillard, F. Mathevet, A-J. Attias, and F. Charra, Langmuir **27**, 10 251 (2011).

[23] J. A. Lipton-Duffin, O. Ivasenko, D. F. Perepichka, and F. Rosei, Small **5**, 592 (2009).
[24] J. Krömer, I. Rios-Carreras, G. Fuhrmann, C. Musch, M. Wunderlin, T. Debaerdemaeker, E. Mena-Osteritz, and P. Bäuerle, Angew. Chem., Int. Ed. **39**, 3481 (2000).
[25] See Supplemental Material at http://link.aps.org/supplemental/10.1103/PhysRevLett.110.056802 for details on data treatment and analysis.
[26] R. Telesca, H. Bolink, S. Yunoki, G. Hadziioannou, P. Th. Van Duijnen, J. G. Snijders, H. T. Jonkman, and G. A. Sawatzky, Phys. Rev. B **63**, 155112 (2001).
[27] M. Bednarz, P. Reineker, E. Mena-Osteritz, and P. Bäuerle, J. Lumin. **110**, 225 (2004).
[28] B. V. Numerov, Mon. Not. R. Astron. Soc. **84**, 592 (1924).
[29] Lord Rayleigh, *Scientific Papers* (Cambridge University Press, Cambridge, England, 1912), Vol. 5, p. 172.
[30] K. R. Hiremath, R. Stoffer, and M. Hammer, Opt. Commun. **257**, 277 (2006).
[31] The cases $(a, b) = (0, 1)$ and (1,0) constitute exceptions where $|Y(\theta)|^2$ is constant.
[32] Note that for a linear wire with a finite potential, the wave functions no longer vanish at the boundaries and they slightly spread out of the wire. This induces small deviations from the parabolic dispersion of the infinite potential, depending on the wire length and potential height.
[33] R. Gleiter, B. Esser, and S. C. Kornmayer, Acc. Chem. Res. **42**, 1108 (2009).